CHAPTER

Structural aspects of inflammasomes forming NOD-like receptors

14

Inga V. Hochheiser and Matthias Geyer
Institute of Structural Biology, University of Bonn, Venusberg-Campus 1, Bonn, Germany

1. Introduction

Inflammasome-forming proteins are systemic receptors of the innate immune system that induce inflammation in response to harmful stimuli, such as pathogens, dead cells, particulate matter, or other irritants [1]. Innate immune cells use germ-line encoded pattern recognition receptors (PRRs) that allow for a broad and rapid initial recognition of the invader and the activation of downstream effector mechanisms counteracting the infection. While most PRRs induce the transcriptional upregulation of proinflammatory effector molecules, members of the AIM2-like receptor (ALR) and NOD-like receptor (NLR) superfamilies upon ligand encounter form multiprotein signaling platforms called inflammasomes. Upon activation, a domino-type queue of pyrin domain (PYD) and caspase activation recruitment domain (CARD) interactions build these supramolecular complexes that are formed by homotypic assemblies leading to filamentous structures. The inflammasomes initiate innate defense and inflammatory responses by activating caspase-1 and pyroptotic cell death in myeloid cells. In this chapter, we describe the inflammasome forming proteins from primary sequence to quaternary structure and correlate their three-dimensional assemblies with cellular function.

2. Inflammasome-forming NOD-like receptors

Canonical inflammasome formation begins with the ligand-induced activation of ALR or NLR sensor proteins, which in turn oligomerize and recruit pro-caspase-1. Proximity-induced autoproteolytic cleavage of the recruited zymogen generates active caspase-1, which subsequently cleaves and thereby activates the proinflammatory cytokines pro-IL-1β and pro-IL-18 [2]. Next to cytokine maturation, caspase-1 induces a proinflammatory type of cell death, called pyroptosis [3,4]. Noncanonical inflammasome formation is caspase-1 independent and involves the direct recognition of cytosolic LPS by human caspase-4 and -5 or murine caspase-11. Upon activation, these caspases oligomerize and induce pyroptosis, but not cytokine maturation [5,6], whereas the two main effector mechanisms of canonical inflammasome formation are cytokine maturation and pyroptosis [4]. Pyroptosis is induced by caspase-mediated proteolytic cleavage of gasdermin D, which results in the release of the

Inflammasome Biology. https://doi.org/10.1016/B978-0-323-91802-2.00022-0

N-terminal effector domain from its autoinhibitory C-terminus and subsequent oligomerization and pore formation in the plasma membrane of the infected host cell [7].

The inflammasome forming PRRs belong either to the ALR but mainly to the NLR superfamily. The human NOD-like receptor superfamily consists of 22 members that share a similar molecular domain architecture comprising of a central NACHT domain and a C-terminal leucine-rich repeat (LRR) domain. The name of the central NACHT domain is derived from the proteins in which it was first identified by bioinformatic analyses, namely NAIP, CIITA, HET-E, and TEP1 [8]. According to their differing N-terminal effector domain, NLRs are subclassified into NLRA (CIITA), NLRB (NAIP), NLRCs (NOD1, NOD2, NLRC3-5), NLRPs (NLRP1-14), and NLRX (NLRX1) [9]. NLRs are multidomain proteins typically 1000 amino acids in size and a molecular weight of 120 kDa, with human NLRP10 at 75 kDa being the smallest and human NLRC5 at 205 kDa being the largest representative. A phylogenetic tree of the NOD module of the 22 human NLRs is shown in Fig. 14.1A.

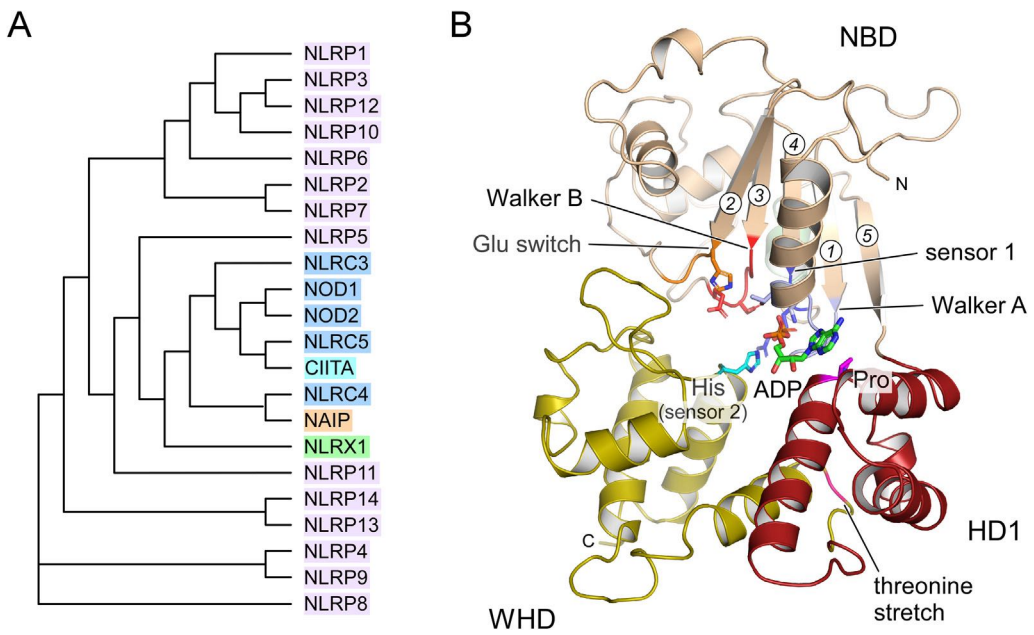

FIGURE 14.1 Characteristics of the NOD module in human NLRs.

(A) Phylogenetic tree of the NOD module of the 22 human NLRs. A sequence segment starting 20 residues upstream of the Walker A motif and ending 20 residues after the conserved His motif (sensor 2) was aligned with Multalin. The phylogram was calculated with Simply Phylogeny. Protein names are color coded according to their NLR subclassification. (B) Conserved sequence motifs in the NOD module. The three subdomains NBD, HD1, and WHD are color coded. The conserved sequence motifs and the ADP nucleotide are displayed in stick representation and labeled using the structure of human NLRP3 (7pzc). The characteristic five-stranded, parallel β-sheet is marked.

3. NOD-like receptors are STAND family ATPases

NOD-like receptors are classified as P-loop NTPases based on the presence of the highly conserved NACHT domain that possesses nucleoside-triphosphatase (NTPase) activity [10]. P-loop NTPases contain a 200−250 aa long ATP binding domain, which encodes two conserved amino acid sequence motifs, namely the Walker A (also phosphate-binding or P-loop) and the Walker B motif that coordinate nucleotide binding and hydrolysis [11,12]. The structure of the P-loop domain is characterized by a three-layered αβα sandwich of repeating β-loop-α units, also known as Rossmann-fold, where the β-strands are arranged in parallel orientation and surrounded by α-helices [13]. P-loop NTPases diversified throughout evolution into the kinase-GTPase (KG) family, where the P-loop and the Walker B motif-containing strand are adjacent to each other, and the "additional strand catalytic E" (ASCE) family, where an additional β-strand between the P-loop and the Walker B motif is inserted [10,14,15]. The β-sheet in ASCE NTPases contains a characteristic parallel β2-β3-β4-β1-β5 topology, where the P-loop (or Walker A motif) is directly following the first β-strand (β1) and the Walker B motif is located on the third β-strand (β3). This ASCE core module is referred to as "nucleotide-binding domain" or NBD [16]. The topology of this family-defining β-sheet is shown in Fig. 14.1B.

NLRs are further classified into the group of "ATPases associated with diverse cellular activities" (AAA+ ATPases), which contains a great variety of proteins implicated in various functions such as DNA replication, protein folding, proteolysis, transcription regulation, and cell division [17]. The primary feature of AAA+ ATPases is the addition of a C-terminal helical lid domain (also called "helical domain 1" or HD1) to the ASCE core module [16]. Based on structure predictions and sequence similarity to the animal apoptosis regulators CED4/Apaf-1 and plant disease resistance proteins, NLRs were further grouped into the "signal transduction ATPases with numerous domains" (STAND) class [10]. STAND ATPases in addition contain a "winged helix domain" (WHD) resulting in a sequential domain architecture of NBD-HD1-WHD [18]. This entity is designated as core "nucleotide-binding oligomerization domain" (NOD) module in STAND ATPases [8,19]. All human NOD-like receptors contain in addition a "helical domain 2" (HD2) as part of this module which completes the C-terminal end of the NACHT domain [20].

4. Sequence motifs in the NOD module

The involvement of STAND ATPases in the formation of large signaling hubs is widely spread across diverse organisms such as plants, nematodes, and mammals. They cover a wide range of activities and often control fundamental cellular processes, including transcription regulation, innate immune responses, and apoptosis [18]. On the basis of biochemical and structural data, STAND ATPases have been proposed to act as binary switches between an "off" and "on" state. In the following, we will refer exclusively to the 22 human NOD-like receptors that are involved in numerous severe and sometimes chronic pathologies.

There are a number of sequence motifs that can be readily inferred from primary sequence alignments. For the most part, they have functional significance and are all located in the conserved NBD-HD1-WHD module of the NLRs. The motifs in the core NOD module are displayed in Fig. 14.1B. The Walker A motif starts at the bottom of β1 with the conserved sequence pattern GxxGxGK(T/S) (where x is any amino acid) in human NLRs [21,22]. The lysine residue coordinates

the β- and γ-phosphate groups of the bound nucleotide, while the hydroxyl group of the threonine or serine residues participates in coordination of the magnesium cation; although a bound magnesium ion has not been identified in any known NLR structure determined to date, presumably due to low binding affinity. The Walker B motif typically reads hhhhDE, where h represents a hydrophobic amino acid, but is degenerated to hhhhDGxDE in human NLRs [22]. It is located on β3 with the hydrophobic residues residing in the β-sheet structure and the two acidic residues at the tip of the β-strand. The glutamic acid in the typical Walker B motif is supposed to coordinate a water molecule that can be activated for an in-line attack of the γ-phosphate of the bound ATP to initialize hydrolysis. In the known NLR structures, the "DGx" residues loop away from the bound nucleotide while the following "DE" motif forms a short 3_{10}-helix with the two acidic residues positioned in face to the terminal phosphate group.

In some AAA+ ATPases, the ATP hydrolysis activity mediated by the Walker B motif is regulated by the "Glu-switch," which is located on the terminal β2-strand of the central β-sheet. The name relates to the observation that the conserved glutamate in the neighbouring Walker B motif can switch from an inactive to an active conformation upon substrate binding [23]. While in the inactive state, the glutamate interacts with a conserved asparagine at the tip of β2, it is switched toward the nucleotide upon binding of a cofactor to the terminal β-strand [24]. This mechanism provides a means to link ATP hydrolysis with substrate interaction, which can also be the oligomerization of multiple subunits in homomeric assemblies. In NLRs, no particular sequence conservation is present at the position of the tip of β2 (which is H260 in NLRP3 or S368 in NLRP1). However, it is noteworthy that some prominent disease mutations such as the R262W CAPS mutation in NLRP3 are in close proximity to this proposed regulatory site.

Sensor 1 is structurally centered between the Walker A and B motifs at the tip of strand β4. Sensor 1 is a conserved feature in AAA+ ATPases and thought to sense the status of the bound nucleotide. This sequence motif is hhhTTR in NLRs, with the first five residues embedded in the β-strand and the basic arginine side chain facing the terminal phosphate group. The motif is succeeded by a tightly packed helix positioned behind the central β-sheet and leading into the final strand β5 [21,22]. In some AAA+ ATPases, sensing of the γ-phosphate shifts the proceeding helix for trans-acting catalysis of ATP hydrolysis in the adjacent molecule. This ATPase-stimulating activity is achieved by a conserved arginine residue, also called Arg-finger, toward the end of the α-helical fold [25]. However, the Arg-finger is missing on helix α4 in NLRs. Instead, a shift of helix α4 upon exchange of the smaller ADP to the larger ATP is thought to induce a conformational rearrangement in the NBD to HD2 subdomain assembly [26].

While all sequence motifs described so far are located in the nucleotide-binding domain (NBD), only one highly conserved residue is found in helical domain 1 (HD1). Initially described as GxP module in STAND ATPases [10], it condenses to a single conserved proline as the first residue of the fourth α-helix in HD1, which interacts with the adenine base of the bound nucleotide. The last structurally and functionally conserved sequence motif in NLRs is Sensor 2 which is comprised of a single histidine residue in the winged helix domain (WHD) [18,22]. Located at the beginning of helix α5 in the WHD, this histidine is facing with its imidazole ring the α- and β-phosphate groups of the bound ADP nucleotide in the structures of NLRC4, NOD2, and NLRP3. However, the motif might not be considered highly conserved as 5 of the 22 human NLRs contain other residues (S, D, V, L) at this position than a histidine. Residues in the vicinity of the motif (FxHxxxQxF) are similarly well conserved [22], possibly due to structural constraint of the helical assembly in the WHD.

5. Domain composition and architecture of NOD-like receptors

The above-described conserved sequence motifs are all contained in the core NOD module composed of subdomains NBD, HD1, and WHD. A prototypic assembly of an NLR with the N-terminal effector domain, the central regulatory NOD module, and the C-terminal sensory LRR domain is shown in Fig. 14.2A.

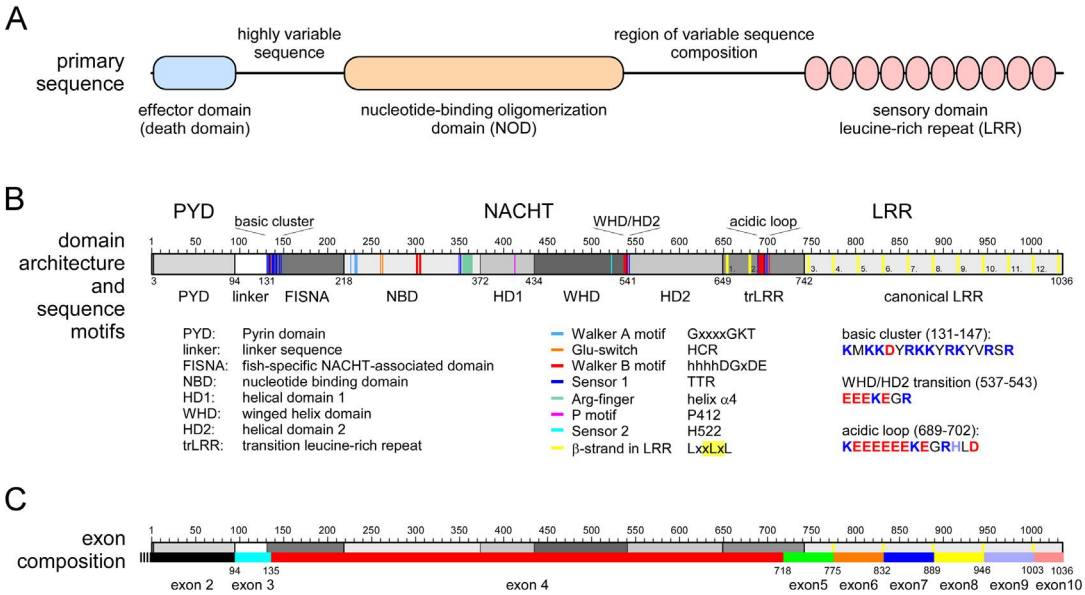

FIGURE 14.2 Domain architecture, sequence motifs, and exon composition of a NOD-like receptor exemplified for human NLRP3.

(A) Archetypical domain composition of a NOD-like receptor as derived from the primary amino acid sequence. At the N-terminus resides an effector domain, which is usually a PYD or CARD with a molecular weight of ~10 kDa. The central "nucleotide-binding oligomerization domain" (NOD) is name-giving to the NLRs and defined as NACHT domain. It is the regulatory domain that determines the oligomerization state of the NLR. At the C-terminus, a variable number of leucine-rich repeats persists that are thought to function as sensory domain. The region between the death and NACHT domain is highly variable in sequence and length for each NLR, whereas the region between the core NACHT domain and the canonical LRRs is less variable in length but most characteristic for each NLR. (B) Domain architecture of human NLRP3 as derived from structural analysis. The region between the PYD and NACHT domain contains a flexible linker sequence and a loosely structured stretch (FISNA), that covers the nucleotide-binding site. The NACHT domain contains the characteristic nucleotide interaction motifs. The LRR region starts with a transition segment, whose LRR composition cannot be easily derived from primary sequence analysis. While this region may have additional regulatory functions, it merges into a canonical part that is thought to contain the sensory function. The NACHT and LRR region is highly structured with only some interspersed flexible loop segments. (C) Exon composition of human NLRP3 (NCBI gene identifier NM_004895.5). Whereas the NACHT and trLRR domains are encoded by one exon only (exon 4), the canonical LRR is made of repetitive exons (exon 5–10) that each contain one 28aa/29aa-tandem repeat.

In all 22 human NLRs, the core NOD module adopts a well-defined structure and on average consists of 322 residues, with only very few amino acid insertions or deletions (standard deviation equals ±10 residues). Only the NLRX1 NOD module is slightly longer with 355 residues, which relates to an insert of 20 amino acids between the first and second α-helix in HD1. The three-layered αβα sandwich of the NBD (typically 155 aa) is followed by a four-helix bundle of the HD1 (∼60 aa) that is continued by a twisted five-helix assembly of the WHD (∼107 aa). The WHD sometimes contains a short β-hairpin loop between the fourth and fifth α-helix as resolved in the crystal structure of NLRC4 [27]. The transition from the NBD to HD1 subdomain is highly structured, although α1 of HD1 starts with multiple charged residues (mostly five, but also six as the D_{351}KDKKK sequence in NLRP6) that could play a role in the coordination of flexible loops in the NLRs. The transition of HD1 to WHD is marked by a long loop that was shown to allow for a 90° rotation between helix α4 of HD1 and helix α1 of WHD upon the activation of the NLR, based on the structures of autoinhibited and activated NLRC4. A stretch of threonines in this loop (T361 in NLRC4 or T438 in NLRP3) marks the rotation point from the inactive to the active conformational transition (Fig. 14.1B).

The NOD module in NLRs is flanked by an additional N-terminal "fish-specific NACHT associated" (FISNA) subdomain and a C-terminal "helical domain 2" (HD2), both of high sequence variability and various length. These two subdomains largely add to the specificity and functional diversity of the receptors and, together with the NOD module, constitute the NACHT domain. They are significantly less well conserved and cannot be easily recognized by computational analyses. The N-terminal FISNA is composed of several helices meandering on the NBD that form a lid for the nucleotide binding site. A rather short variant of this subdomain is found in the *C. elegans* protein CED-4 with only 43 residues (aa 108−151) [28], whereas it can be longer than 100 amino acids as for example in NLRP1. In human NLRP3, the FISNA is supposed to contain an additional activation loop close to the transition to the NBD, as the phosphorylation of two serine residues S_{198}PVS$_{201}$PI was shown to stimulate NLRP3 activation [29]. A diagram of the domain architecture and the localization of conserved sequence motifs is exemplarily shown for NLRP3 in Fig. 14.2B.

At the C-terminal end, the NACHT domain is completed by the HD2 subdomain that exists in many STAND ATPases and in all NLRs [18,20]. This segment is most diverse and not conserved at a sequence level, although it contains a similar fivefold up-down-up-down-up helical scaffold in the known structures of NLRC4, NOD2, and NLRP3, with the incoming "up"-helices at the outer rim of the overall structure. Characteristic features in this segment contribute to the specificity of the protein. For example, in NLRC4, the third helix ("up") continues into a long, extended loop that binds into the concave side of the succeeding LRR structure before returning into an elongated straight helix ("down") of 26 residues [27]. This segment is supposed to support the autoinhibition of NLRC4 by interacting with the NBD and LRR domains. In NOD2, two short helical elements are built in between the first and second canonical helix instead, which are however of unknown functional significance yet [30].

In the NLR protein structures known today, the HD2 merges seamlessly into a cryptic leucine-rich repeat fold that is usually not recognized as LRR by computational methods. In this segment, the β-strands and α-helices are typically longer than in the bona fide LRRs and may not follow the strict LxxLxL consensus sequence expected for this repeat structure [31]. In addition, they may be interspersed with an additional loop section, which renders secondary structure predictions difficult. Due to its flexible nature, we have termed this segment "transition LRR" (or trLRR). Together, HD2 and trLRR can easily encompass 250 to 300 residues (e.g., 275 in NOD2). Of note, the HD2 and trLRR region that appeared as terra incognita in previous computational analyses are sometimes also referred

to as "NACHT-associated domain" or NAD in early publications (e.g., Mayor et al. [32]). Toward the C-terminus, the transition LRR is continuing into a bona fide canonical LRR fold (cnLRR) that adopts the typical horseshoe-curved shape by the parallel assembly of β-strand/α-helical repeats [31]. For many NLRPs, the cnLRR domain is composed of a rigorous alteration of 28-/29-residue tandem repeats, as seen, for example, for the RNase inhibitor protein [33]. In NLRP3, as in some other NLRPs, each tandem repeat is encoded by an individual exon, which is shown in Fig. 14.2C. In contrast, succession of homogenous 28-residue repeats exists for NOD1, NOD2, NLRC3, or CIITA, each of which is encoded by one exon (for a detailed analysis see Hoss et al. [34]). Most human NLRs contain 11 to 15 LRR repeats, while only NLRC5 is significantly longer with more than 40 repeats, whereas NLRP10 is missing a canonical LRR domain.

The N-terminus of the NLR fold is established by an effector domain. This can be either a "Pyrin domain" (PYD), as in the 14 NLRPs, or a "caspase recruitment domain" (CARD) as found in NLRC4, NLRC5, NOD1, and NOD2, the latter even having two consecutive CARDs. PYDs and CARDs are both six-helical bundle domains of approximately 90 and 95 residues, respectively, but with different topologies [35]. Both domains are able to form filamentous structures, either as a right-handed three-start helical filament of ∼6.6 PYD subunits per helix turn or as a left-handed one-start helical filament of four CARD subunits per turn. For NLRP3, NLRP6, ASC, and AIM2, homomeric PYD filament structures have been determined [36−40], as for the CARD filaments of NLRP1, NLRC4, and ASC [41−43]. Yet, not all PYDs or CARDs of the NLRs are able to form filamentous structures or even proceed into homotypic transitions to ASC or caspases. The N-terminal regions of NLRC3, NLRX1, and CIITA remain unclear, only for CIITA an acidic transcriptional activation domain preceding the NACHT domain has been proposed. NAIP finally contains three consecutive BIR domains ("baculovirus inhibitor of apoptosis protein repeat") at its N-terminus, the approximately 80 residues of which consist of a short three-stranded antiparallel β-sheet and five surrounding helices coordinated by a zinc-finger.

The N-terminal effector domains are connected through a linker of variable length and low sequence complexity to the FISNA, respectively, NACHT domain. The linker length ranges from very few amino acids in NLRPs 4, 9, 10, and 11 to more than 200 residues in NLRP1, showing the variability in the molecular arrangement of these NLRs. In NLRP3, the 40 amino acid linker is encoded by a single exon, again pointing to the unusual but intriguing correlation between exon usage and domain composition in NLRs.

6. Conformational states of NLRs from inactive to active

Our current understanding of the transition between the inactive and the active state of a NOD-like receptor is largely shaped by the available structures of NLRC4 [27,44−47]. A major breakthrough was the determination of the crystal structure of the autoinhibited conformation of NLRC4 using a mouse variant protein construct in which the CARD domain was deleted [27]. This protein is monomeric in solution and adopts a profile like a question mark. Only 2 years later, the first active structures of murine NLRC4 have been determined by single particle cryogenic electron microscopy (cryo-EM), showing disc-like assemblies of 10−12 subunits with the highest probability and structural resolution for a homomeric 11-mer [44,45]. NLRC4 activation was achieved by addition of the sensor protein NAIP2 and its ligand PrgJ from the bacterial type III secretion system (T3SS) of *Salmonella*.

Spirals of flagellin-induced NAIP5/NLRC4 multimers were also observed, but the activating ligand could not be identified in the electron density maps of either structure [46]. Model reconstructions revealed a ~90° hinge rotation between the HD2 and WHD subdomains of the NACHT domain, resulting in new surface accessibilities of the NLR oligomerization domains. It took another 2 years that a *Legionella* flagellin bound NAIP5–NLRC4 inflammasome was resolved in which the circular assembly was kept half open, allowing for the identification of the seeding moiety at one end [47]. It shows how flagellin binds to NAIP5 and unfurls the protein for subsequent NLRC4 recruitment and activation, leading to self-propagating oligomerization and completion of a caspase-1 recruitment platform.

Based on these structures, we provide a general schematic of the proposed conformational changes and oligomeric assemblies upon NLR activation which is displayed in Fig. 14.3. The domain architecture of a prototypical NLR is shown with the individual subdomains color-coded at the top. In a simplistic scheme, the receptor protein resides in an autoinhibited, ADP-bound inactive conformation

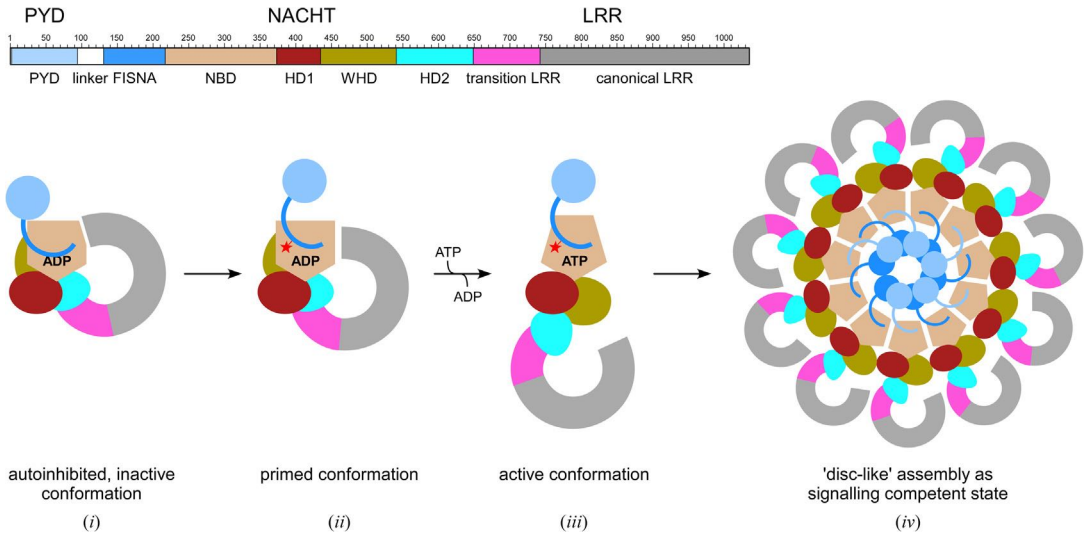

FIGURE 14.3 Schematic of the proposed activation mechanism of an inflammasome-forming NLR.

Simplistic conformational states of NLR activation. The typical domain architecture of a NOD-like receptor is displayed at the *top*, shown here for human NLRP3. (*i*) In the basal state, the receptor protein resides in an autoinhibited, ADP-bound inactive conformation. (*ii*) Upon a priming step, which can be, for example, a phosphorylation event (*red asterisk*), the protein relieves its autoinhibited conformation and the nucleotide binding site is becoming accessible. (*iii*) The loss of autoinhibition allows exchange of the bound nucleotide to ATP, which is thought to induce a conformational change in the nucleotide-binding domain (NBD). The interaction of sensor 1 with the bound nucleotide leads to a rotation of subdomains WHD/HD2 relative to NBD/HD1. (*iv*) In its active conformation, the NLR protein is able to assemble into an oligomeric quaternary structure, mostly driven by NBD, HD1, and WHD interactions. This assembly was shown for NAIP/NLRC4 to be a circular disc-like structure. The helical assembly of the effector domain (either PYD or CARD) in the central hub of this disc is thought to be the seed for ASC, respectively, caspase, filament formation and displays the signaling competent state.

in the resting state (*i*). Upon a priming step, which can be, for example, a phosphorylation event (red asterisk), the protein relieves its autoinhibited conformation and the nucleotide binding site is becoming accessible, resulting in the primed state (*ii*). The abolition of autoinhibition allows for the release of ADP and the exchange of the bound nucleotide for ATP. The interaction of sensor 1 with the bound nucleotide presumably induces a conformational change in the nucleotide-binding domain (NBD). This leads to a rotation of the subdomains WHD/HD2 relative to NBD/HD1, resulting in the active conformation (*iii*). In its active conformation, the NLR protein is able to associate into an oligomeric assembly, which was shown for NAIP/NLRC4 to be an 11-mer disc-like structure. This disc-like assembly is the signaling-competent state (*iv*) that acts as a seed for inflammasome formation. The helical assembly of the effector domain (either PYD or CARD) in the center of the disc is thought to be the nucleation seed for ASC filament formation and caspase maturation.

7. Structures of inactive inflammasomal proteins

The crystal structure of murine NLRC4-ΔCARD bound to ADP (PDB accession code 4kxf) determined at 3.2 Å resolution is the prototype for an inactive, autoinhibited mammalian NLR [27]. The structure reveals the paramount importance of the HD2 and trLRR domains in gaining molecular specificity for this protein family. Contacts between a phosphorylated serine residue (pS533) of HD2 with the concave site of the LRR and marginal interactions between the C-terminal end of the LRR and the NBD result in closure of the solenoid structure and provide a mechanism for autoinhibition (Fig. 14.4A). A 31 residue insert between helices α3 and α4 of HD2 compared to NLRP3 reaches out to the LRR with pS533 mediating multiple electrostatic interactions contributing to the closure in this inactive state. Another insert of 23 residues in the trLRR domain directly following the second β-strand of the LRR instead has been deleted for crystallization purposes. This structure also showed for the first time how closely the NACHT subdomains interact with each other including the FISNA, that forms a lid on the ADP nucleotide with the characteristic 5-arm NBD β-sheet being extended by two further antiparallel strands from the FISNA.

The crystal structure of rabbit NOD2 in an ADP-bound state (5irn, 2.34 Å resolution) consolidated our view on the autoinhibited conformation of NLRs [30]. NOD2 is thought to recognize muramyl dipeptide, a bacterial cell wall fragment, for activation. Single-nucleotide polymorphisms in the NOD2 gene have been associated with chronic inflammatory disorders such as Crohn's disease, Blau syndrome, and early-onset sarcoidosis [48]. For crystallization, the N-terminal tandem CARD effector domains, which are required for recruiting the kinase RIPK2 through CARD−CARD interactions, have been truncated (Fig. 14.4B). While also this structure represents an inactive state, a superimposition with NLRC4 reveals that an insert segment between the first and second canonical helix in the HD2 of NOD2 positions the beginning of the transition LRR outward, leading to a different angle of the LRR relative to the NACHT domain compared to NLRC4. As also the number of β-strands in the LRR of NOD2 is reduced with 11 compared to 16 in NLRC4, a closing of the LRR to the NBD is not maintained (Fig. 14.4C). Nonetheless, the FISNA covers the nucleotide-binding site of the bound ADP and a free exchange to ATP is prohibited.

The paradigm of monomeric NLRs in the inactive state was recently challenged by the cryo-EM structures of human and mouse NLRP3, with both studies utilizing full-length proteins [49,50] (Fig. 14.5A and B). The human sample was produced in *Sf9* insect cells and purified by affinity

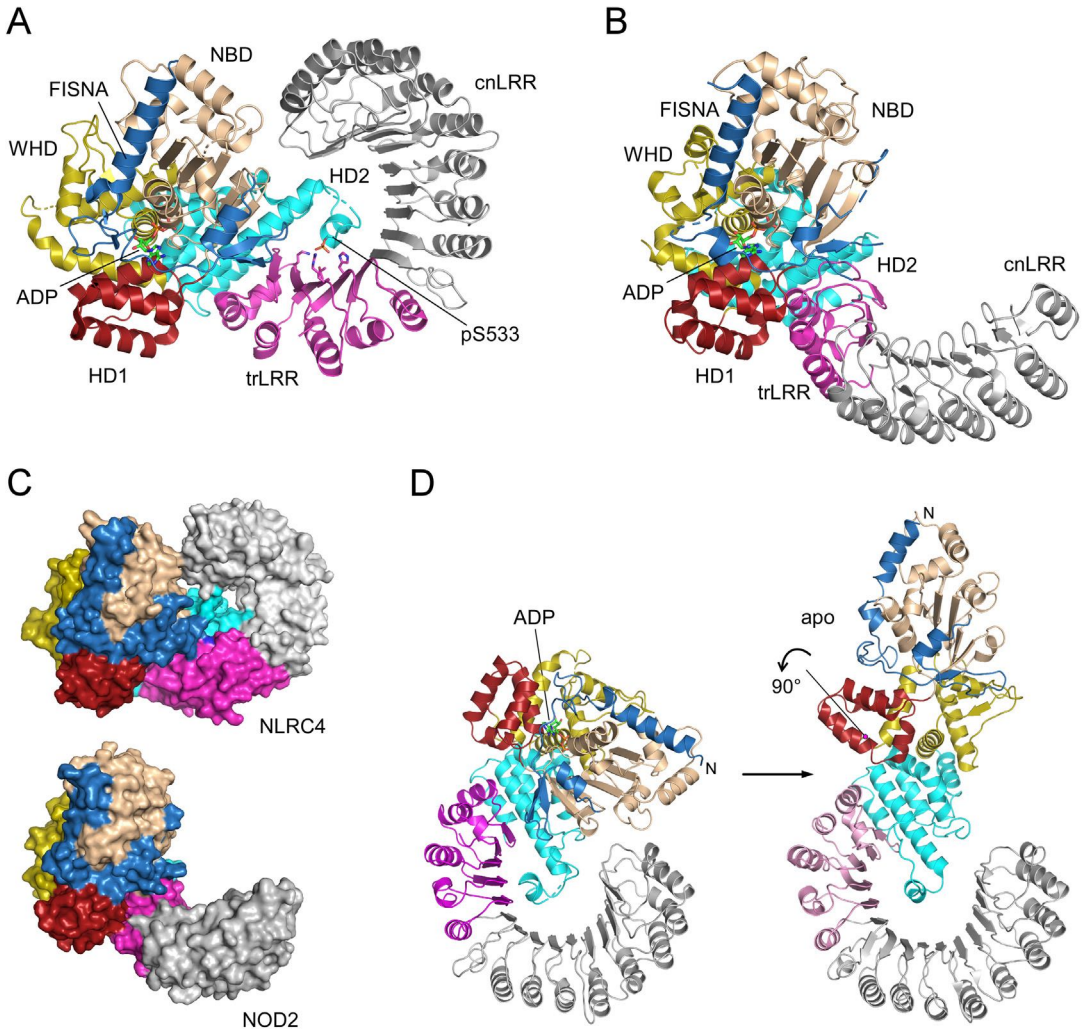

FIGURE 14.4 Autoinhibited or inactive NLR structures of NLRC4, NOD2, and NLRP3.

(A) Crystal structure of murine NLRC4-ΔCARD bound to ADP (4kxf). The electrostatic interaction of phospho-S533 in an elongated helix of HD2 with residues K611, T665, R667, and H693 of trLRR keeps the protein in an autoinhibited conformation. (B) Crystal structure of rabbit NOD2-ΔCARDs bound to ADP (5irn) shown in the same orientation of NBD/HD1 subdomains as for NLRC4. The shorter trLRR and cnLRR section compared to NLRC4 is in a partly open conformation. (C) Surface displays showing the tight assembly of subdomains in NLRC4 and the partly open conformation in NOD2. (D) Conformational transition from autoinhibited NLRC4•ADP to active NLRC4 in the apo state when oligomerizing to NAIP5 (4kxf and 6b5b, chain B). The structures are aligned to the WHD-HD2-LRR region. The pivot point for the rotation between HD1 and WHD is marked with a dot.

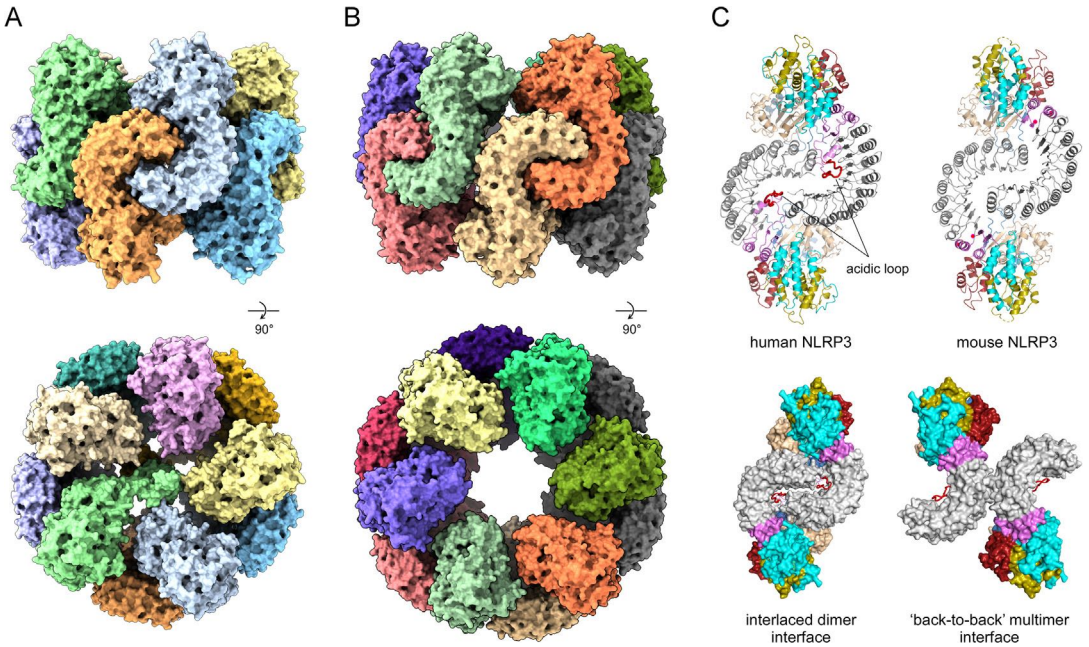

FIGURE 14.5 Structures of inactive NLRP3 from humans and mice.

(A) Cryo-EM structure of human NLRP3 bound to ADP and the inhibitor CRID3/MCC950 (7pzc). The assembly of NLRP3 appears as a pentamer of dimers, with a twofold rotational symmetry between two LRR domains interlocked with their concave sites, and a fivefold rotational symmetry of the apical NACHT domains. One PYD dimer is in addition buried inside the cavity of the sphere. (B) Cryo-EM structure of murine NLRP3 in an apo state after purification with dATP (7lfh). Here, NLRP3 appears as a hexamer built from similarly interlaced LRR dimers. The inner cavity is supposed to accommodate all 12 PYDs, although not built into the density map. (C) While the acidic loop mediates the dimer interaction of the interlaced LRR domains in human NLRP3, this region is not resolved in the structure of murine NLRP3 (*top*). The dimer interface of intertwined LRRs (*left*) and of the LRR "back-to-back" interface, building the multimeric assemblies (*right*) are displayed at the *bottom*.

chromatography as MBP fusion protein in the presence of ADP before TEV cleavage to remove the tag. Initial reconstructions at a resolution of 8−11 Å revealed an overall spherical structure with a pentameric assembly at the polar sites and a meander ring along the equator. Addition of the NLRP3-specific inhibitor MCC950/CRID3 significantly stabilized the structure without inducing any conformational changes, in line with its function as an antagonist. Structural analysis at 3.9 Å resolution showed that ADP-bound, human NLRP3 is a decamer composed of homodimers of intertwined LRR domains that assemble back-to-back as pentamers (7pcz; Fig. 14.5A). The NACHT domain is located at the apical axis of this spherical structure, but intermolecular interactions within adjacent NACHT domains that would further stabilize the quaternary assembly were not observed. While most PYDs are not resolved in the structure, one PYD dimer is formed inside the spherical LRR cage. Molecular contacts forming the homodimer assembly of NLRP3 are made between the interlocked

concave sites of two opposing LRRs (Fig. 14.5C). The interaction is mediated by an acidic loop extending from the transition LRR domain and binding into the concave surface of the canonical LRR by multiple electrostatic interactions. The acidic loop sequence is at the tip of an LRR-mismatching region of 42 residues that interrupts the conventional fold at the second β-strand and is a characteristic of NLRP3. Each C-terminus of the LRRs is thus entirely buried by homomeric complement leaving it unresolved how C-terminal tagging, e.g., with immunepitopes, can maintain this autoinhibited conformation.

The structure of mouse NLRP3 in an inactive state instead showed hexa- to octamer assemblies of dimeric NLRP3 being similarly formed by homomeric face-to-face LRR contacts [50]. Here, the protein was expressed in HEK293T cells in the presence of dATP suggesting that an active state was converted to an inactive conformation. However, a bound nucleotide was not resolved in the cryo-EM structure. The full-length mouse NLRP3 expression construct was designed as FLAG-mScarlet-tagged fusion protein and affinity purified with anti-FLAG M2 affinity gel before TEV cleavage for tag removal. The three species with 6-, 7-, and 8-fold symmetry were equally distributed indicating heterogeneity in the oligomerization state, but the resolution was best for the 6-fold double-ring structure purified with dATP (7lfh, 4.2 Å) that is displayed in Fig. 14.5B. The LRRs showed the similar interlaced domain association, but although the acidic loop in the transition LRR is also present in mice, this loop region was not resolved in the cryo-EM structure (Fig. 14.5C). This could indicate either conformational differences between mouse and human NLRP3, which could affect, e.g., binding to effector proteins such as NEK7 (see below), or conformational transitions in the loop region that may have resulted from the use of dATP. Of note, human and mouse NLRP3 are of 1036 and 1033 amino acid length, respectively, and share 83% sequence identity and 90% sequence similarity. There was additional density visible for the N-terminal PYDs in the cage formed by the two NACHT-LRR rings but due to the absence of any specific features in the density maps the PYDs were not modeled into the structure. This observation suggests that the PYDs are shielded within the LRR cage to avoid nucleating the adaptor protein ASC.

8. Structure of active inflammasome-forming NLRs

The structure of an active NLR has been shown until to date only for murine NLRC4 and its activating co-receptors NAIP2 or NAIP5 (3jbl, 5aj2, 6b5b). While active NLRC4 in its oligomerization prone state is able to form circular discs or even endless spirals [44–46], activation of NAIP5 with the bacterial substrate protein flagellin from *Legionella pneumophila* was resolved without applying symmetry and at nonsaturating NLRC4 stoichiometries, leaving the disc-formation unclosed [47]. This allowed the reconstruction of a single NAIP5 subunit at the initiating side of the growing circle, uniquely identified by its bulky BIR domains and bound to a single flagellin monomer (Fig. 14.6A). The NAIP5 "donor" surface unfurls by flagellin binding to recruit the cognate "acceptor" surface of NLRC4 by complementary polar and hydrophobic interactions mainly in the NBD, HD1, and WHD domains (Fig. 14.6B). These oligomerization surfaces of NLRC4 become accessible only upon the transition into an active conformation (Fig. 14.4D). This self-propagating oligomerization mechanism recruits and activates additional NLRC4 subunits for inflammasome assembly, but is unable to interact with the acceptor surface of NAIP5, leaving the receptor for bacterial pathogens as the nucleation seed at the starting side of this assembly. Density of low resolution was resolved at the center of the circular

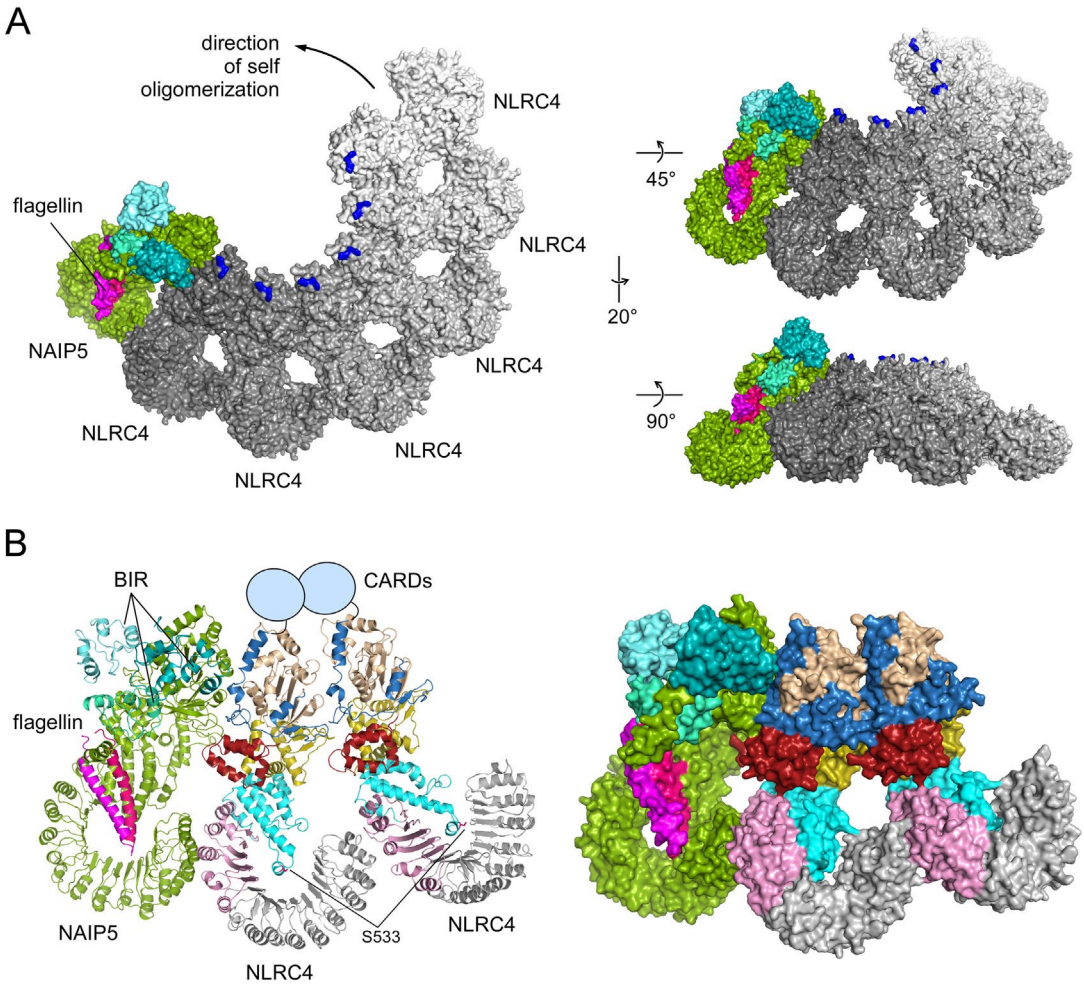

FIGURE 14.6 Structure of the active NAIP5—flagellin—NLRC4 inflammasome.

(A) Structure of murine NAIP5 bound to flagellin from *Legionella pneumophila*, seeding for the disc-like assembly of multiple NLRC4 subunits (6b5b). The direction of oligomerization in this self-propagating mechanism is indicated. The N-termini of the FISNA of the murine NLRC4 subunits are colored *blue* indicating the position of the CARDs. (B) Ribbon display (*left*) of a NAIP5—NLRC4—NLRC4 trimer, induced by flagellin binding to NAIP5 (6b5b). The three N-terminal BIR domains of NAIP5 are labeled. The position of the none-phosphorylated S533 residue in NLRC4 is indicated. The putative position of the CARD domains is shown as spheres. The surface display shows the tight subdomain interaction of the oligomeric assembly (*right*).

NLRC4 structures in proximity to the NBD domains, indicating the proposed position of the CARDs as a hub for caspase-1 recruitment (Fig. 14.6B). However, it remains unclear how many CARD domains are minimally required to form a nucleation seed for caspase binding and maturation. Since only four domains form one layer in the CARD filament structure, ring closure of the NLRC4 NACHT-LRR domains seems not required to achieve a signaling competent state.

Based on the assembly of 11 NLRC4 subunits into a planar disc, a model for an active NLRP3 inflammasome in complex with the kinase NEK7 has been proposed [51]. The mitotic serine/threonine kinase NEK7 is thought to license the assembly and activation of the NLRP3 inflammasome during interphase of the cell cycle [52]. The cryo-EM structure of an inactive human NLRP3 complex with the kinase NEK7 was determined to 3.8 Å resolution (6npy) [51]. Modeling of an active NLRP3 conformation based on the ~90° HD1 to WHD rotation seen for NLRC4 allowed assembly of multiple NLRP3−NEK7 protomers without steric hindrance. In this 11-fold planar disc, the C-terminal lobe of NEK7 interacts with the convex LRR surface of the neighboring NLRP3 molecule stabilizing this assembly. However, while the iconic picture of an active NLRP3−NEK7 disc-like structure has been well perceived [36,53], this model still awaits experimental validation.

9. Downstream effectors of the NLR nucleation seed

A first insight into the downstream signaling events of active NLRs has been provided by the structural investigation of several different PYD and CARD filaments [36−43]. The cyro-EM structures of the human $NLRP6^{PYD}$ (6ncv), $AIM2^{PYD}$ (6mb2, 7k3r), and $NLRP3^{PYD}$ (7pzd) filaments show a remarkably similar symmetry in rotation and axial rise per subunit as determined first for the human ASC^{PYD} filament structure (3j63) [36−40]. Like the ASC^{PYD} filament, they display a right-handed three-start helical symmetry with approximately 6.5 subunits per helical turn, solidifying a concept of a homotypic transition between the upstream receptor protein to downstream adaptor elongation in the course of ASC speck formation. In the filament structures, the PYD subunits are arranged in a hexagonal assembly creating three asymmetric interfaces that interact with six adjacent PYDs. The interface sides form unique surfaces at the filament ends, designated as A- and B-end, respectively, according to the a- and b-side residues that assemble at both ends [36].

The directionality of the homotypic receptor-to-adaptor transition has been addressed for NLRP6, AIM2, and NLRP3 employing different methodologies. For NLRP6, the binding energy between a modeled $NLRP6^{PYD}$ to ASC^{PYD} transition was determined to be more favorable if the b-side residues of NLRP6 interacted with the a-side residues of ASC [38]. Similarly, molecular dynamics simulations revealed the more favorable energy levels for an interaction between the top of the $AIM2^{PYD}$ filament (corresponding to its B-end) with the bottom of the ASC^{PYD} filament (corresponding to its A-end) [40]. Unidirectional transitions from a $NLRP3^{PYD}$ to an ASC-mCherry filament were identified by negative stain EM, using a seeding titration assay [54]. This experimental approach revealed that the elongation of ASC filament formation occurs exclusively at the B-end of the preformed $NLRP3^{PYD}$ filament, using cryo-EM analysis for the determination of the filament directionality [36]. A PYD filament covering a model of the homotypic transition from $NLRP3^{PYD}$ to ASC^{PYD} is shown in Fig. 14.7A. Together, these observations shape our understanding of the NLR nucleation seed as a unidirectional signaling platform for ASC speck formation that in the next instance involves homotypic CARD-domain interactions with pro-caspase-1.

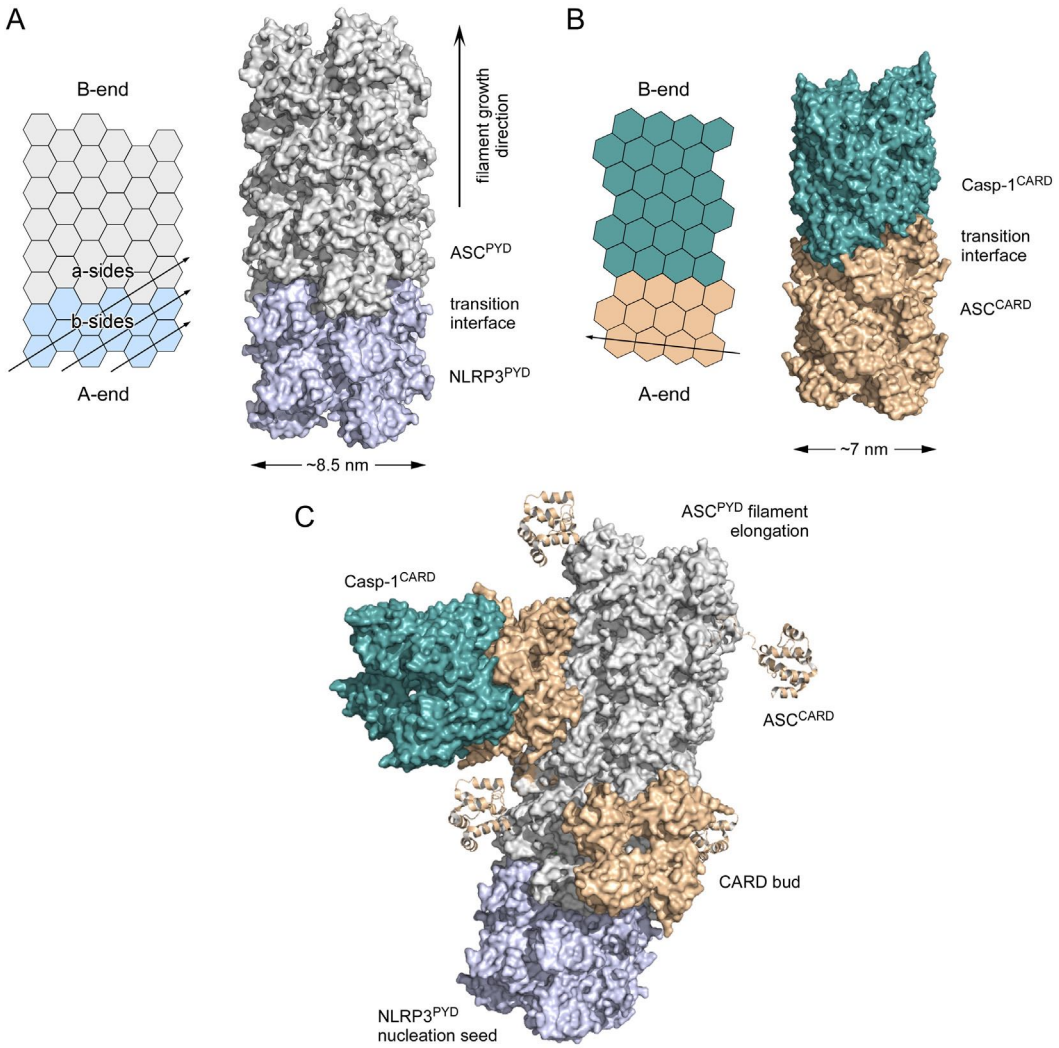

FIGURE 14.7 Filament structures in the ASC speck inflammasome.

(A) Homotypic transition from an NLRP3^{PYD} filament nucleation seed to ASC^{PYD} filament elongation (7pzd and 3j63). A cartoon of the right-handed three-start helix is shown *left* with the A- and B-end of the interfaces indicated. The growth directionality of the filament transition toward the B-end is indicated. (B) Transition of a CARD filament from ASC^{CARD} seeds to caspase-1^{CARD} elongation (6n1h and 5fna). The CARD filament is a left-handed one-start helix of approximately 4 subunits per turn, while the PYD filament has approximately 6.5 subunits per turn. (C) Model of the core ASC speck filament structures. Launched by an NLRP3^{PYD} nucleation seed, ASC^{PYD} domains elongate the filament in a self-propagating assembly mechanism. ASC^{CARDs} assemble on the ASC^{PYD} filament surface to form small buds for caspase-1^{CARD} prolongation. Both filaments grow on the b-sides for homotypic elongation.

The cryo-EM structures of the ASC^{CARD} (6n1h), the $NLRC4^{CARD}$ (6n1i), and the caspase-1^{CARD} (5fna) filaments further unraveled the molecular mechanisms driving ASC speck formation [43,55]. These filamentous structures share a left-handed one-start helical symmetry with roughly 4 subunits per turn (Fig. 14.7B). The helical symmetry parameters (rotation and axial rise per subunit) of the CARD filaments of ASC, NLRC4, and caspase-1 are nearly identical, again indicating a template−adaptor mechanism, where CARD buds of ASC or NLRC4 form the nucleation seeds for pro-caspase-1^{CARD} elongation. Similar as in PYD filaments, CARD filament formation is mediated by three types of asymmetric interfaces between single CARD subunits, generating unique surfaces at the CARD filament ends and therefore different interaction surfaces for potential adaptor binding. Unidirectionality of nucleation seed to adaptor transition was demonstrated for ASC^{CARD} and $NLRC4^{CARD}$ mediated Caspsase-1^{CARD} polymerization, where nanogold labeled ASC and NLRC4 was only detected on one end of the nucleated caspase-1^{CARD} filament [43]. The predicted buried surface area was greater for a modeled transition in which ASC and NLRC4 used their b-sided CARD filament end for recruitment of the a-sided caspase-1^{CARD} filament compared to the reverse interactions. This was later confirmed by the structure of an engineered ASC^{CARD}-caspase-1^{CARD} octamer, that was shown to assemble in the same manner [42]. These observations reveal the dynamics of homotypic filament formation and have implications for the possible interference by antibodies or small molecules at the filament growing site. A model of the core filament structures of an ASC speck with a PYD stem and CARD buds is shown in Fig. 14.7C.

10. Conclusions

Our understanding of NOD-like receptor structures and conformational transitions has only just begun. There are many questions that remain to be answered to unravel the function of these important receptors of the innate immune system. Some emerging structural and mechanism-related questions are: How are NLRs regulated, and in particular, how are they activated? What enables nucleotide exchange from ADP to ATP? How does ATP hydrolysis contribute to NLR regulation? What is the quaternary state of inactive/resting NLRs, are they mostly monomeric or also in oligomeric assemblies? What is the minimally required number of PYDs or CARDs to become a nucleation seed for downstream signaling? Are there antagonistic NLRs that counteract agonistic NLRs, or also protagonistic NLRs as is NAIP for NLRC4? It goes without saying that this plethora of questions is only complementary to the functional characterizations of NLRs in cells in terms of tissue specificity, yield, localization, and much more.

Gaining these insights will only lead to the ultimate question as of how targeted inhibition of NLRs can be achieved to combat inflammatory diseases. The alike domain composition of different NLRs suggests that a similar cleft, as is the binding site for MCC950/CRID3 in NLRP3, is contained in all of them. In addition, their sequence diversity indicates that each site may be unique to each NLR, raising hopes for specific targeting of each receptor. However, the functional consequences of locking this site for the proposed conformational rotation between the HD1 and WHD subdomains that occurs upon activation need to be individually investigated for each NLR. These questions open up a great perspective for future analyses of human NLRs in health and disease.

Acknowledgments

M.G. is funded by the Deutsche Forschungsgemeinschaft (DFG, German Research Foundation) under Germany's Excellence Strategy—EXC2151—390873048.

References

[1] H. Guo, J.B. Callaway, J.P.-Y. Ting, Inflammasomes: mechanism of action, role in disease, and therapeutics, Nat. Med. 21 (2015) 677–687.
[2] P. Broz, V.M. Dixit, Inflammasomes: mechanism of assembly, regulation and signalling, Nat. Rev. Immunol. 16 (2016) 407–420.
[3] K. Schroder, J. Tschopp, The inflammasomes, Cell 140 (2010) 821–832.
[4] M. Lamkanfi, V.M. Dixit, Mechanisms and functions of inflammasomes, Cell 157 (2014) 1013–1022.
[5] N. Kayagaki, S. Warming, M. Lamkanfi, et al., Non-canonical inflammasome activation targets caspase-11, Nature 479 (2011) 117–121.
[6] J. Shi, Y. Zhao, Y. Wang, et al., Inflammatory caspases are innate immune receptors for intracellular LPS, Nature 514 (2014) 187–192.
[7] X. Liu, Z. Zhang, J. Ruan, et al., Inflammasome-activated gasdermin D causes pyroptosis by forming membrane pores, Nature 535 (2016) 153–158.
[8] E.V. Koonin, L. Aravind, The NACHT family—a new group of predicted NTPases implicated in apoptosis and MHC transcription activation, Trends Biochem. Sci. 25 (2000) 223–224.
[9] M. Saxena, G. Yeretssian, NOD-like receptors: master regulators of inflammation and cancer, Front. Immunol. 5 (2014) 327.
[10] D.D. Leipe, E.V. Koonin, L. Aravind, STAND, a class of P-loop NTPases including animal and plant regulators of programmed cell death: multiple, complex domain architectures, unusual phyletic patterns, and evolution by horizontal gene transfer, J. Mol. Biol. 343 (2004) 1–28.
[11] C. Puchades, C.R. Sandate, G.C. Lander, The molecular principles governing the activity and functional diversity of AAA+ proteins, Nat. Rev. Mol. Cell Biol. 21 (2020) 43–58.
[12] T. Ogura, A.J. Wilkinson, AAA+ superfamily ATPases: common structure–diverse function, Genes Cells 6 (2001) 575–597.
[13] K.E. Medvedev, L.N. Kinch, R. Dustin Schaeffer, et al., A fifth of the protein world: Rossmann-like proteins as an evolutionarily successful structural unit, J. Mol. Biol. 433 (2021) 166788.
[14] D.D. Leipe, Y.I. Wolf, E.V. Koonin, L. Aravind, Classification and evolution of P-loop GTPases and related ATPases, J. Mol. Biol. 317 (2002) 41–72.
[15] D.D. Leipe, E.V. Koonin, L. Aravind, Evolution and classification of P-loop kinases and related proteins, J. Mol. Biol. 333 (2003) 781–815.
[16] J.P. Erzberger, J.M. Berger, Evolutionary relationships and structural mechanisms of AAA+ proteins, Annu. Rev. Biophys. Biomol. Struct. 35 (2006) 93–114.
[17] M. Ammelburg, T. Frickey, A.N. Lupas, Classification of AAA+ proteins, J. Struct. Biol. 156 (2006) 2–11.
[18] O. Danot, E. Marquenet, D. Vidal-Ingigliardi, E. Richet, Wheel of life, wheel of death: a mechanistic insight into signaling by STAND proteins, Structure 17 (2009) 172–182.
[19] N. Inohara, G. Nuñez, The NOD: a signaling module that regulates apoptosis and host defense against pathogens, Oncogene 20 (2001) 6473–6481.
[20] J. Maharana, D. Panda, S. De, Deciphering the ATP-binding mechanism(s) in NLRP-NACHT 3D models using structural bioinformatics approaches, PLoS One 13 (2018) e0209420.
[21] P.I. Hanson, S.W. Whiteheart, AAA+ proteins: have engine, will work, Nat. Rev. Mol. Cell Biol. 6 (2005) 519–529.
[22] M. Proell, S.J. Riedl, J.H. Fritz, et al., The nod-like receptor (NLR) family: a tale of similarities and differences, PLoS One 3 (2008) e2119.

[23] X. Zhang, D.B. Wigley, The "glutamate switch" provides a link between ATPase activity and ligand binding in AAA+ proteins, Nat. Struct. Mol. Biol. 15 (2008) 1223−1227.
[24] P. Wendler, S. Ciniawsky, M. Kock, S. Kube, Structure and function of the AAA+ nucleotide binding pocket, Biochim. Biophys. Acta 1823 (2012) 2−14.
[25] T.V. Seraphim, W.A. Houry, AAA+ proteins, Curr. Biol. 30 (2020) R251−R257.
[26] T. Ogura, S.W. Whiteheart, A.J. Wilkinson, Conserved arginine residues implicated in ATP hydrolysis, nucleotide-sensing, and inter-subunit interactions in AAA and AAA+ ATPases, J. Struct. Biol. 146 (2004) 106−112.
[27] Z. Hu, C. Yan, P. Liu, et al., Crystal structure of NLRC4 reveals its autoinhibition mechanism, Science 341 (2013) 172−175.
[28] S. Qi, Y. Pang, Q. Hu, et al., Crystal structure of the *Caenorhabditis elegans* apoptosome reveals an octameric assembly of CED-4, Cell 141 (2010) 446−457.
[29] N. Song, Z.-S. Liu, W. Xue, et al., NLRP3 phosphorylation is an essential priming event for inflammasome activation, Mol. Cell 68 (2017) 185−197.e6.
[30] S. Maekawa, U. Ohto, T. Shibata, K. Miyake, T. Shimizu, Crystal structure of NOD2 and its implications in human disease, Nat. Commun. 7 (2016) 11813.
[31] K. Park, B.W. Shen, F. Parmeggiani, et al., Control of repeat-protein curvature by computational protein design, Nat. Struct. Mol. Biol. 22 (2015) 167−174.
[32] A. Mayor, F. Martinon, T. De Smedt, V. Pétrilli, J. Tschopp, A crucial function of SGT1 and HSP90 in inflammasome activity links mammalian and plant innate immune responses, Nat. Immunol. 8 (2007) 497−503.
[33] B. Kobe, J. Deisenhofer, Crystal structure of porcine ribonuclease inhibitor, a protein with leucine-rich repeats, Nature 366 (1993) 751−756.
[34] F. Hoss, J.L. Mueller, F. Rojas Ringeling, et al., Alternative splicing regulates stochastic NLRP3 activity, Nat. Commun. 10 (2019) 3238.
[35] H.H. Park, Structural analyses of death domains and their interactions, Apoptosis 16 (2011) 209−220.
[36] I.V. Hochheiser, H. Behrmann, G. Hagelueken, et al., Directionality of PYD filament growth determined by the transition of NLRP3 nucleation seeds to ASC elongation, Sci. Adv. 8 (2022) eabn7583.
[37] A. Lu, V.G. Magupalli, J. Ruan, et al., Unified polymerization mechanism for the assembly of ASC-dependent inflammasomes, Cell 156 (2014) 1193−1206.
[38] C. Shen, A. Lu, W.J. Xie, et al., Molecular mechanism for NLRP6 inflammasome assembly and activation, Proc. Natl. Acad. Sci. USA 116 (2019) 2052−2057.
[39] A. Lu, Y. Li, Q. Yin, et al., Plasticity in PYD assembly revealed by cryo-EM structure of the PYD filament of AIM2, Cell Discov 1 (2015) 15013.
[40] M. Matyszewski, W. Zheng, J. Lueck, et al., Distinct axial and lateral interactions within homologous filaments dictate the signaling specificity and order of the AIM2-ASC inflammasome, Nat. Commun. 12 (2021) 2735.
[41] Q. Gong, K. Robinson, C. Xu, et al., Structural basis for distinct inflammasome complex assembly by human NLRP1 and CARD8, Nat. Commun. 12 (2021) 188.
[42] L.R. Hollingsworth, L. David, Y. Li, et al., Mechanism of filament formation in UPA-promoted CARD8 and NLRP1 inflammasomes, Nat. Commun. 12 (2021) 189.
[43] Y. Li, T.M. Fu, A. Lu, et al., Cryo-EM structures of ASC and NLRC4 CARD filaments reveal a unified mechanism of nucleation and activation of caspase-1, Proc. Natl. Acad. Sci. USA 115 (2018) 10845−10852.
[44] Z. Hu, Q. Zhou, C. Zhang, et al., Structural and biochemical basis for induced self-propagation of NLRC4, Science 350 (2015) 399−404.
[45] L. Zhang, S. Chen, J. Ruan, et al., Cryo-EM structure of the activated NAIP2-NLRC4 inflammasome reveals nucleated polymerization, Science 350 (2015) 404−409.

[46] C.A. Diebolder, E.F. Halff, A.J. Koster, E.G. Huizinga, R.I. Koning, Cryoelectron tomography of the NAIP5/NLRC4 inflammasome: implications for NLR activation, Structure 23 (2015) 2349−2357.
[47] J.L. Tenthorey, N. Haloupek, J.R. López-Blanco, et al., The structural basis of flagellin detection by NAIP5: a strategy to limit pathogen immune evasion, Science 358 (2017) 888−893.
[48] R. Caruso, N. Warner, N. Inohara, G. Núñez, NOD1 and NOD2: signaling, host defense, and inflammatory disease, Immunity 41 (2014) 898−908.
[49] I.V. Hochheiser, M. Pilsl, G. Hagelueken, et al., Structure of the NLRP3 decamer bound to the cytokine release inhibitor CRID3, Nature 604 (2022) 184−189.
[50] L. Andreeva, L. David, S. Rawson, et al., NLRP3 cages revealed by full-length mouse NLRP3 structure control pathway activation, Cell 184 (2021) 6299−6312.e22.
[51] H. Sharif, L. Wang, W.L. Wang, et al., Structural mechanism for NEK7-licensed activation of NLRP3 inflammasome, Nature 570 (2019) 338−343.
[52] H. Shi, Y. Wang, X. Li, et al., NLRP3 activation and mitosis are mutually exclusive events coordinated by NEK7, a new inflammasome component, Nat. Immunol. 17 (2016) 250−258.
[53] A. Tapia-Abellán, D. Angosto-Bazarra, C. Alarcón-Vila, et al., Sensing low intracellular potassium by NLRP3 results in a stable open structure that promotes inflammasome activation, Sci. Adv. 7 (2021) eabf4468.
[54] I.V. Hochheiser, M. Geyer, An assay for the seeding of homotypic pyrin domain filament transitions, Methods Mol. Biol. 2523 (2022) 197−207.
[55] A. Lu, Y. Li, F.I. Schmidt, et al., Molecular basis of caspase-1 polymerization and its inhibition by a new capping mechanism, Nat. Struct. Mol. Biol. 23 (2016) 416−425.